Supplementary Information

Synthesis of a Homologous Series of Trialkyl Arsines (C_3-C_{12}) and Applications of Arsenic Triiodide as a Synthetic Precursor

Carolina B. P. Ligiéro, [a] ***Marcos A. S. Francisco,***[a] ***Michelle S. Gama,***[b] ***Carlos A. Carbonezi,***[b] ***Isabela C. L. Leocadio,***[b] ***Wladmir F. de Souza***[b] ***and Pierre M. Esteves*** *,[a]

[a]*Instituto de Química, Universidade Federal do Rio de Janeiro, Av. Athos da Silveira Ramos, 149, CT, A-629, Cidade Universitária, 21941-909 Rio de Janeiro-RJ, Brazil*

[b]*PETROBRAS/CENPES, Ilha do Fundão, Quadra 7, 21949-900 Rio de Janeiro-RJ, Brazil*

General

All the solvents were dried with pre-activated 3 Å molecular sieves (Sigma-Aldrich, St. Louis, USA) and distilled before use. Grignard reactions were conducted with magnesium turnings as received (Sigma-Aldrich, St. Louis, USA). Tetrahydrofuran was supplied from Tedia (Fairfield, USA), alkyl halides, and the butyllithium solution were supplied from Sigma-Aldrich (St. Louis, USA) or prepared by methods described in the literature. The arsenic oxide was obtained from Vetec (Duque de Caxias, Brazil).

GC-MS analyses were performed in a Shimadzu GCMS-2010 with a 30 m DB-5 column and helium as the carrier gas. The oven temperature was adjusted according to the volatility of the compounds. Fragmentograms were obtained with the electron impact (EI) method.

The GC × GC-TOFMS system was a Pegasus 4D (Leco, St. Joseph, MI, USA), which is an Agilent Technologies 6890 GC (Palo Alto, CA, USA) equipped with a secondary oven and a non-moving quadjet dual-stage modulator. Data acquisition and processing were carried out using ChromaTOF software version 4.5 (LECO Corp., St. Joseph, MI). The GC column set consisted of a DB-5, 5%-phenyl-95%-methylsiloxane (60 m, 0.25 mm i.d., 0.25 µm df) as the first dimension (1D) and a DB 17 ms (Austin, Texas, USA), a mid-polar column virtually equivalent to (50%-phenyl)-methylsiloxane (2.0 m, 0.18 mm i.d., 0.18 µm df) as the second dimension (2D). The primary oven temperature program was 40 °C for 0.5 min, ramp at 1.5 °C min^{-1} to 200 °C, and them ramp at 10 °C min^{-1} to 250 °C (for 5 min). The secondary oven temperature program had a temperature 10 °C higher than that of the primary one. The carrier gas flow rate was 1.0 mL min^{-1} using helium. The modulation period was 10 s with a 1.65 s hot pulse duration and a 15 °C modulator temperature offset *versus* the primary oven temperature. The MS transfer line was held at 280 °C, and the TOFMS was operated in the electron ionization mode with a collected mass range of *m/z* 35-400. The ion source temperature was 230 °C, the detector was operated at 1370 V, the applied electron energy was 70 eV, and the acquisition rate was 100 spectra s^{-1}.

Powder X-ray diffraction was conducted at a Bragg-Brentano Ultima IV diffractometer from Rigaku. The experiment employed a Cu Kα (40 kV, 20 mA) source with Kβ filter, DivSlit: ½ degree; DivHLSlit: 10 mm; SctSlit: 8.0 mm; step: 0.01 degree.

^{1}H NMR and ^{13}C NMR were obtained with Bruker Advance 400 MHz or 500 MHz, in solutions of $CDCl_3$.

*e-mail: pesteves@iq.ufrj.br

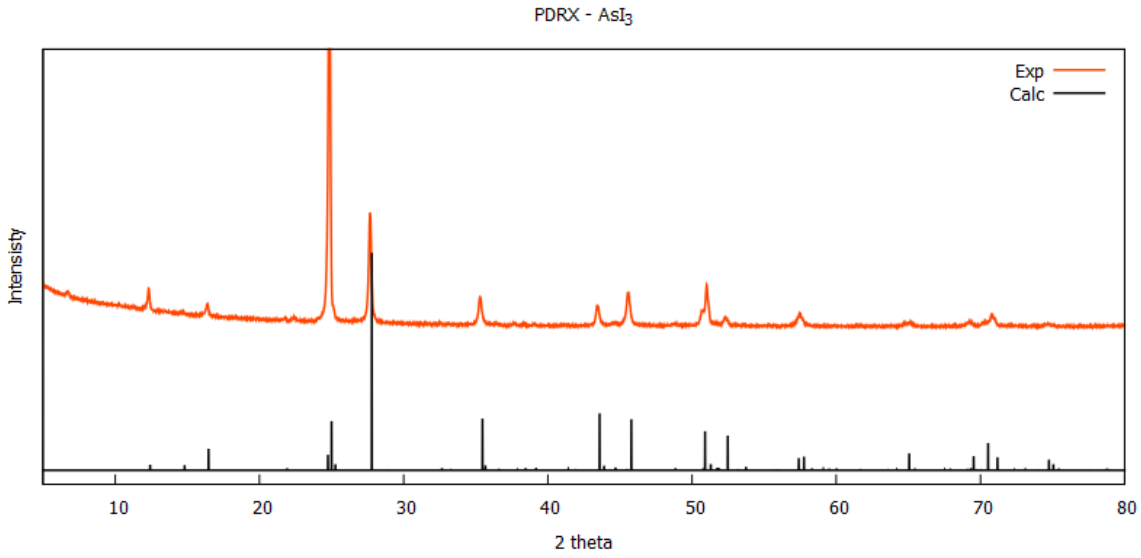

Figure S1. Powder diffractogram of AsI_3.

Powder diffractogram of AsI_3 was compared with that calculated from the single crystal data (Figure S1).[1-3] Powder diffractogram was predicted from the single crystal data of Cambridge Crystallographic Data Center identifier (ICSD 23003) with the software PLATON v. 1.19.[2] The position of the Bragg reflections indicates that the present method provides a good quality product. Some reflections present higher intensities caused by preferential orientation, which is a consequence of the favorable growth of the 001 face by the stronger interactions As···I. These interactions were mapped with red points over the Hirshfeld surface (Figure S2, Hirshfeld surface calculated from the single crystal data of Cambridge Crystallographic Data Center identifier (ICSD 23003) with the software Crystal Explorer v. 17.5).[4]

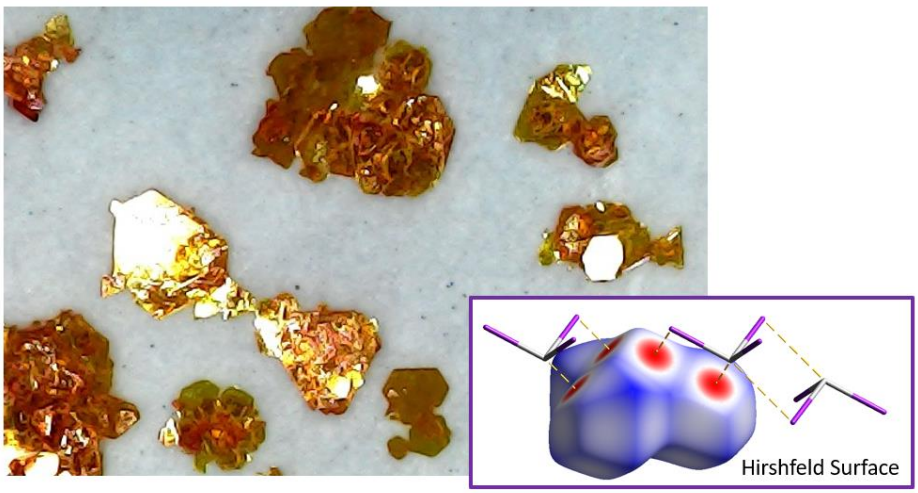

Figure S2. Crystals of AsI_3 and Hirshfeld surface highlighting some intermolecular interactions (plotted with the normalized contact distance, d_{norm} from −0.2255 to 0.98701).

Preparation of tributyl arsine (TBAs)

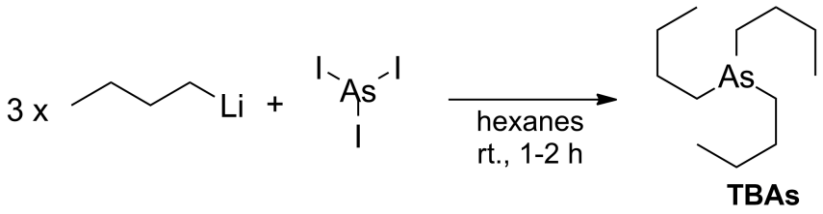

Scheme S1. Synthesis of TBAs.

In a two neck bottom rounded flask with magnetic stirring and inert atmosphere, there were added 19.7 g (42.4 mmol) of arsenic iodide and 36 mL of anhydrous hexane; a red-orange suspension was obtained. At room temperature, 54 mL (135 mmol, 3.2 eq.) of a solution of *n*-BuLi (2.5 mol L^{-1} in hexanes) were added dropwise. After 1 h of stirring, the red-orange suspension was consumed and a pale yellow solid was formed when the reaction was stopped with a small amount of water. The solvent was removed under vacuum and TBAs was purified by distillation under vacuum. Pure tributylarsine was obtained as a colorless oil, in 26% yield (2.7 g, 10.98 mmol) based on AsI_3.

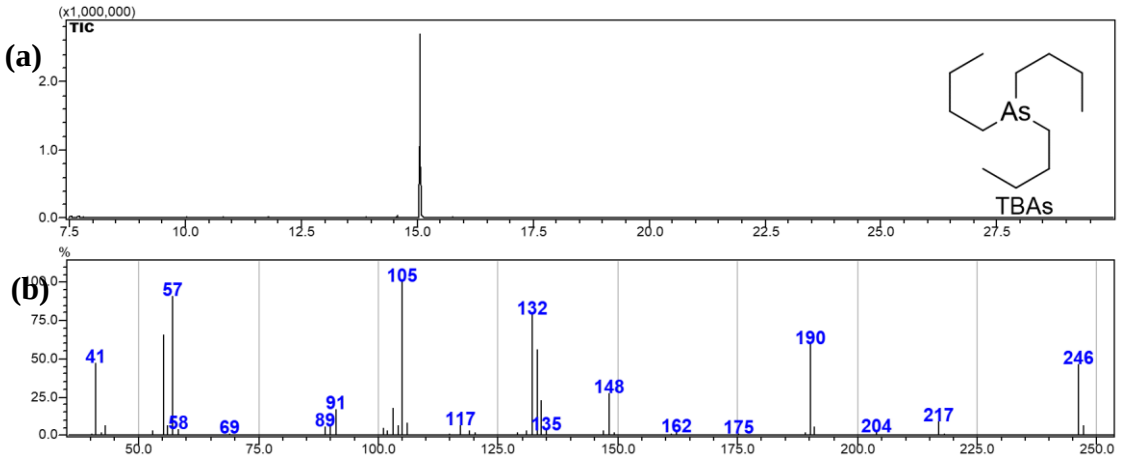

Figure S3. Chromatogram (a) and fragmetogram (b) of TBAs.

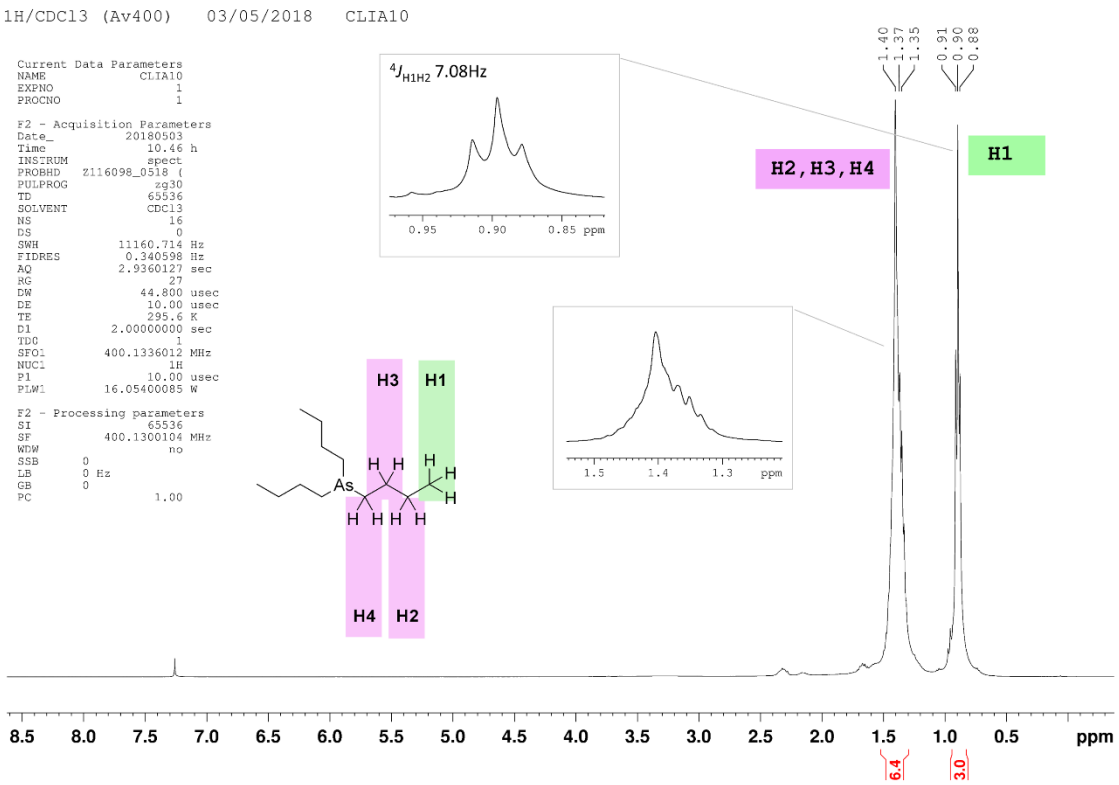

Figure S4. ^{1}H NMR spectrum (400 MHz, $CDCl_3$) of TBAs.

Preparation of tripropyl arsine (TPAs)

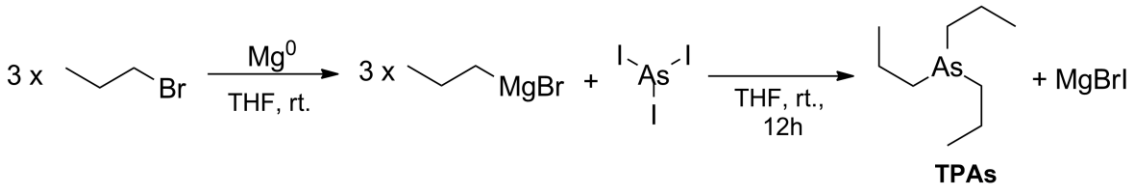

Scheme S2. Synthesis of TPAs.

Metallic magnesium (528 mg, 22 mmol) and 50 mL of dry tetrahydrofuran were added to a two neck bottom rounded flask equipped with magnetic stirring, condenser, and inert atmosphere. Then, 2 mL (22 mmol) of propyl bromide were added over reaction media. After the magnesium consumption, 3.32 g (7.3 mmol) of AsI_3 were added portionwise. The reaction was maintained under an inert atmosphere and with stirring until the orange solid was replaced by a pale yellow precipitate (about 6 h). Then, a saturated solution of ammonium chloride was added and extracted with ethyl ether (3 × 10 mL). The solid was filtered off and the organic layer was dried over magnesium sulfate and analyzed with GC-MS.

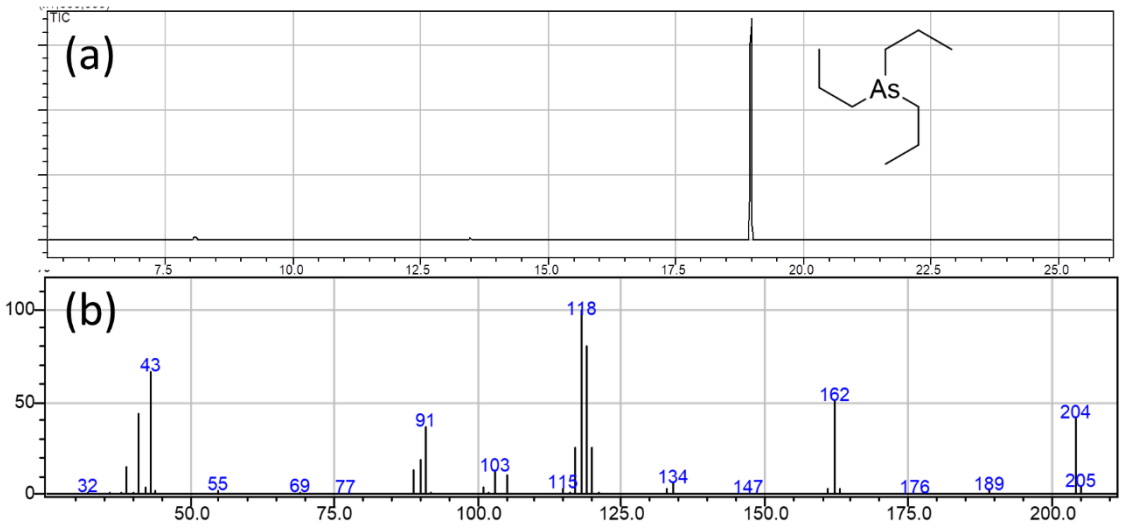

Figure S5. Chromatogram (a) and fragmetogram (b) of TPAs.

Preparation of tributyl arsenite (TBOAs)

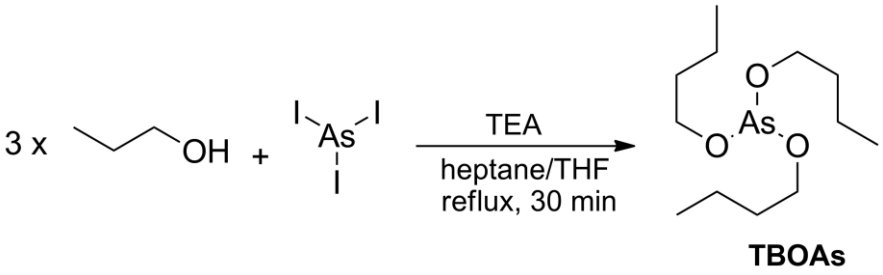

Scheme S3. Synthesis of TBOAs.

To a two-neck bottom rounded flask with magnetic stirring and inert atmosphere, 7.87 g (17.3 mmol) of AsI_3, 20 mL of heptane, and 20 mL of THF were added, resulting in an orange-red suspension (Figure S6c). In another flask, a solution of 4.7 mL (52 mmol, 3 eq.) of 1-butanol, 7.2 mL (52 mmol, 3 eq.) of triethylamine, and 10 mL of heptane were prepared and, then, added to reaction media. Reaction media was heated to reflux and the reaction was completed after some minutes. The pale yellow (Figure S6d) precipitate was removed by filtration and the solvent evaporated under vacuum. Tributyl arsenite was extracted from the crude product with dichloromethane and analyzed by GC-MS(EI). The molecular ion was not observed at *m/z* 294.

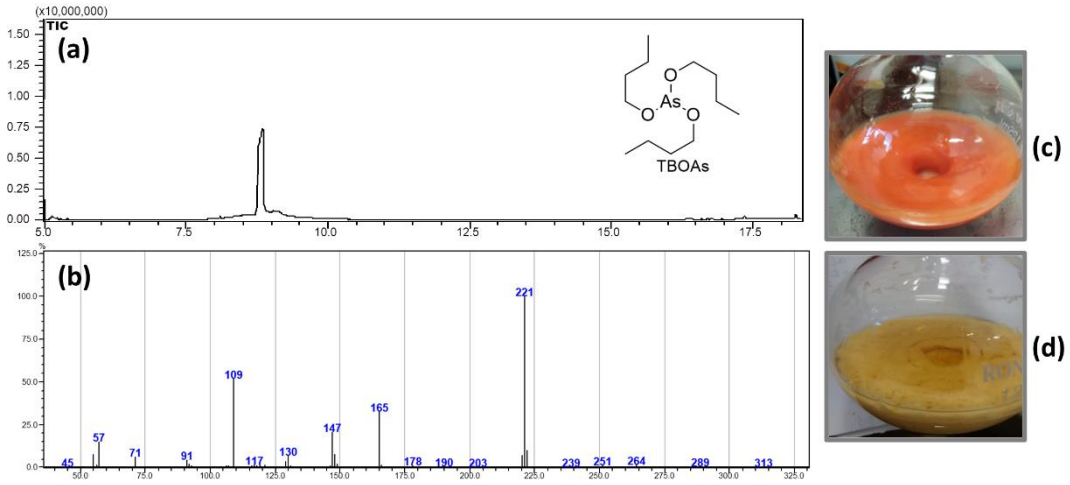

Figure S6. Chromatogram (a) and fragmentogram (b) of TBOAs. Reaction media at the beginning (c) and the end (d) of the synthesis.

Preparation of tripropyl trithioarsenite (TPSAs)

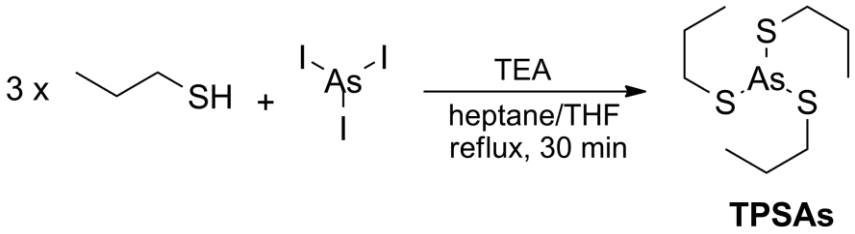

Scheme S4. Synthesis of TPSAs.

Arsenic triiodide (4.4 g, 9.66 mmol) and 10 mL of dry tetrahydrofuran were added to a two-neck round bottom flask equipped with magnetic stirring, condenser, and inert atmosphere. Apart, a solution of 2.6 mL (29 mmol, 3 eq.) of 1-propanethiol, 3.9 mL (29 mmol, 3 eq.) of dry triethylamine in 5 mL of dry heptane were prepared and, then, added to the reaction media. The reaction was warmed until reflux and after some minutes the orange precipitate (Figure S7c) turned pale yellow (Figure S7d). The solid fraction was removed by filtration and the product was purified by fractionated vacuum distillation. The product was obtained as a yellow oil (Figure S7e). Tripropyl trithioarsenite is air-sensible and decomposes to dipropyl disulfide and arsenic oxide.

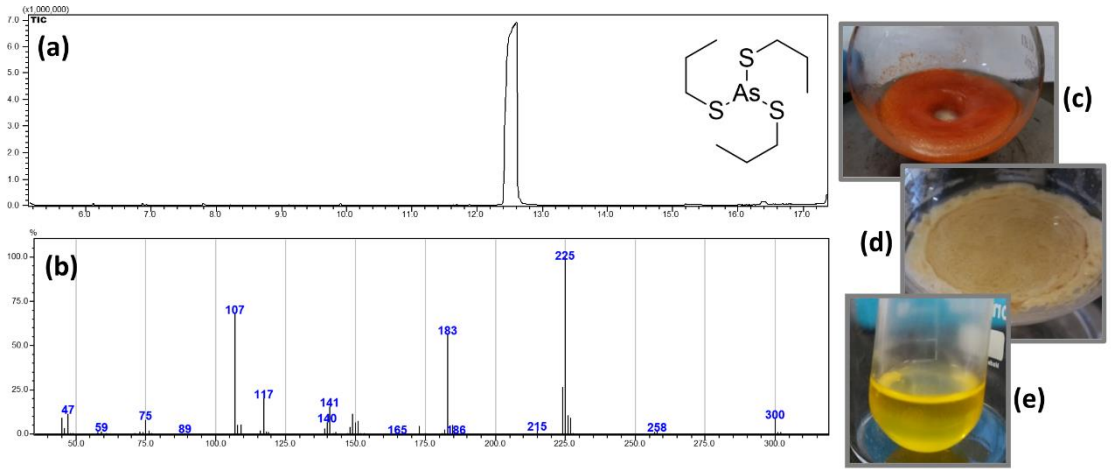

Figure S7. Chromatogram (a) and fragmetogram (b) of TPSAs. Reaction media at the beginning (c) and the end (d) of the synthesis; (e) isolated product.

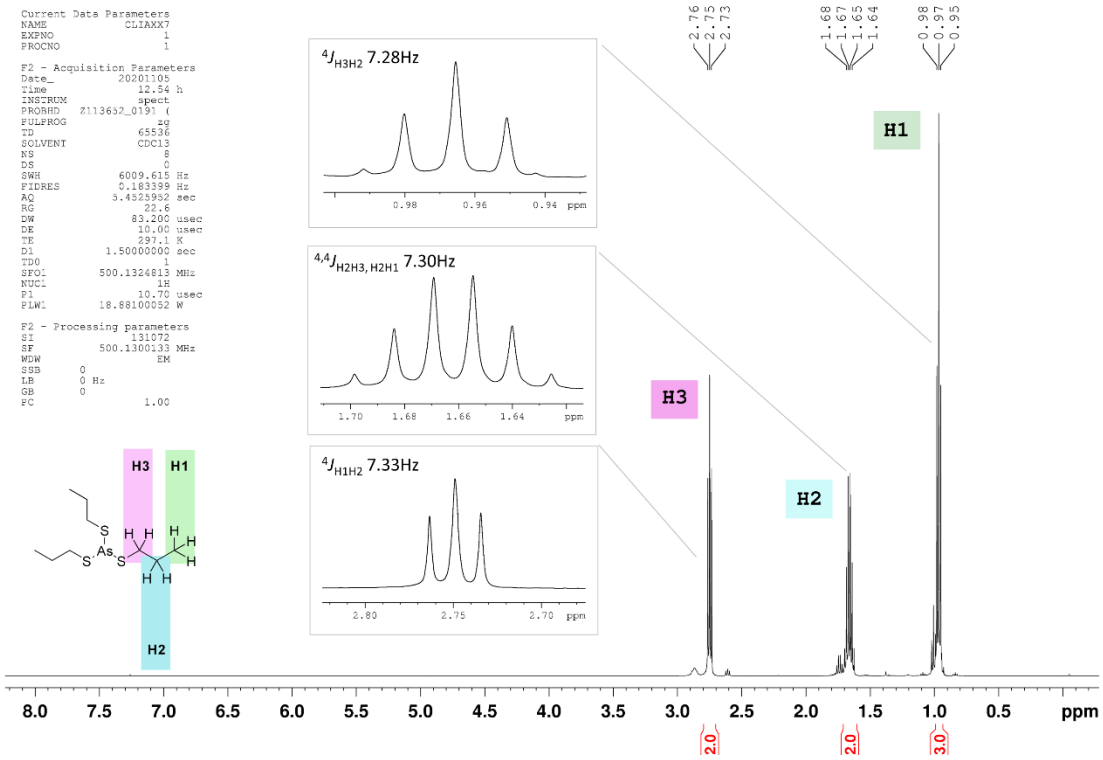

Figure S8. ^{1}H NMR spectrum (500 MHz, $CDCl_3$) of TPSAs.

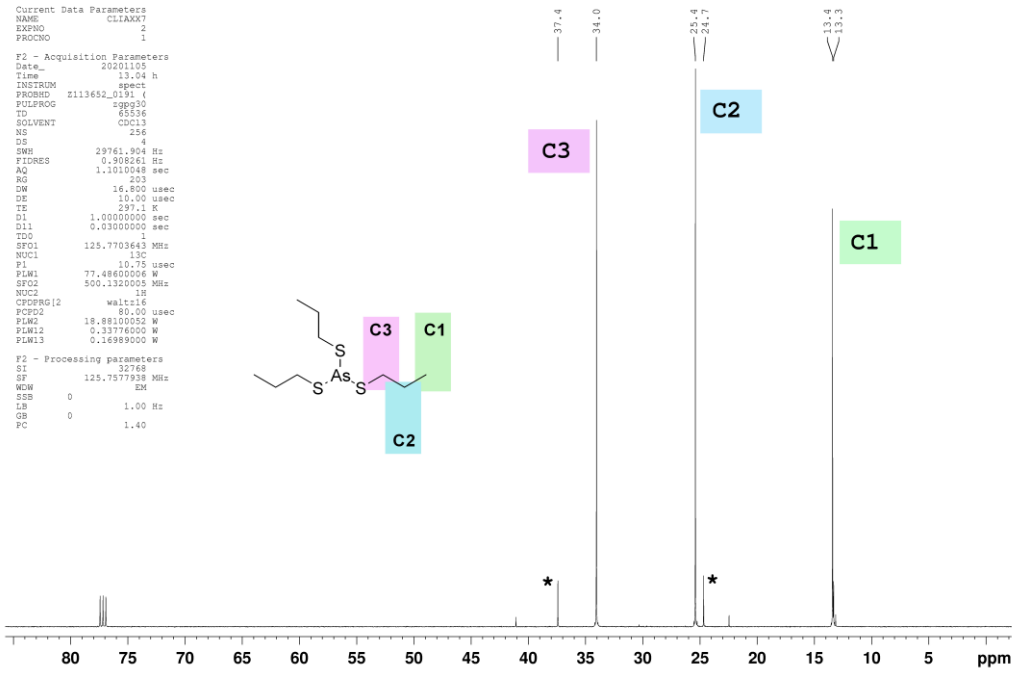

Figure S9. ^{13}C NMR spectrum (125 MHz, $CDCl_3$) of TPSAs. *Decomposition products.

Trialkyl arsines homologous series: fragmentograms

GC × GC-TOFMS total ion count (TIC) mode chromatogram exhibits trialkyl arsines, tetrahydrofuran (reaction solvent), and some linear alkanes like pentane and octane, formed as byproducts from Wurtz coupling of the Grignard reagents (Figure S10). Arsines are in the emphasized section.

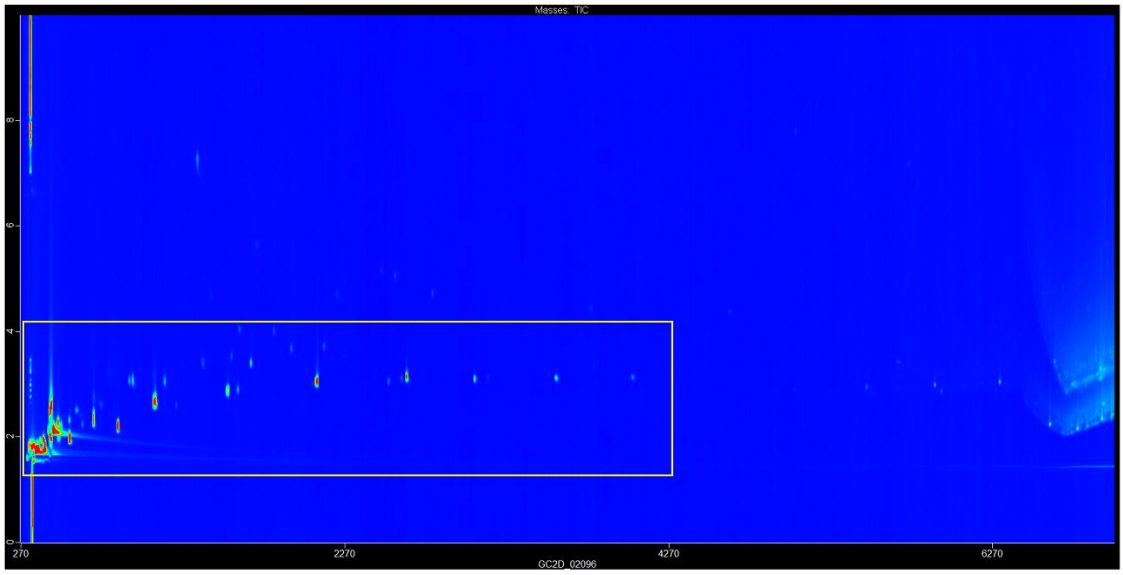

Figure S10. GC × GC-TOFMS (total ion count).

GC × GC-TOFMS with ions selection displays the trialkyl arsines homologous series (Figure S11).

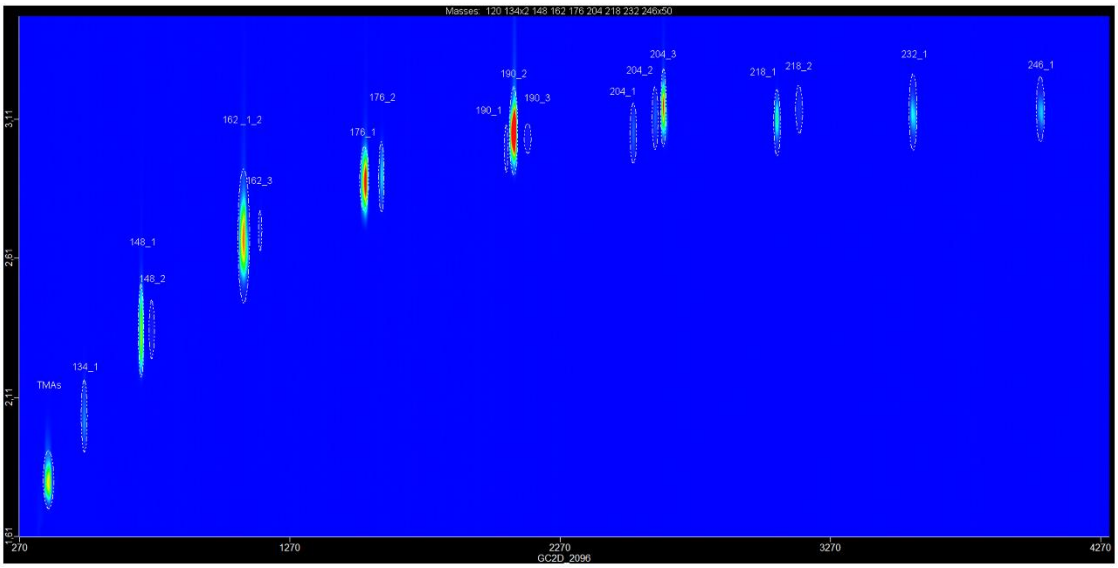

Figure S11. GC × GC-TOFMS highlighting arsine series (*m/z* selected: 120; 134 × 2; 148; 162; 176; 204; 218; 232; 246 × 50).

Trialkyl arsines predicted are displayed in Figure S12.

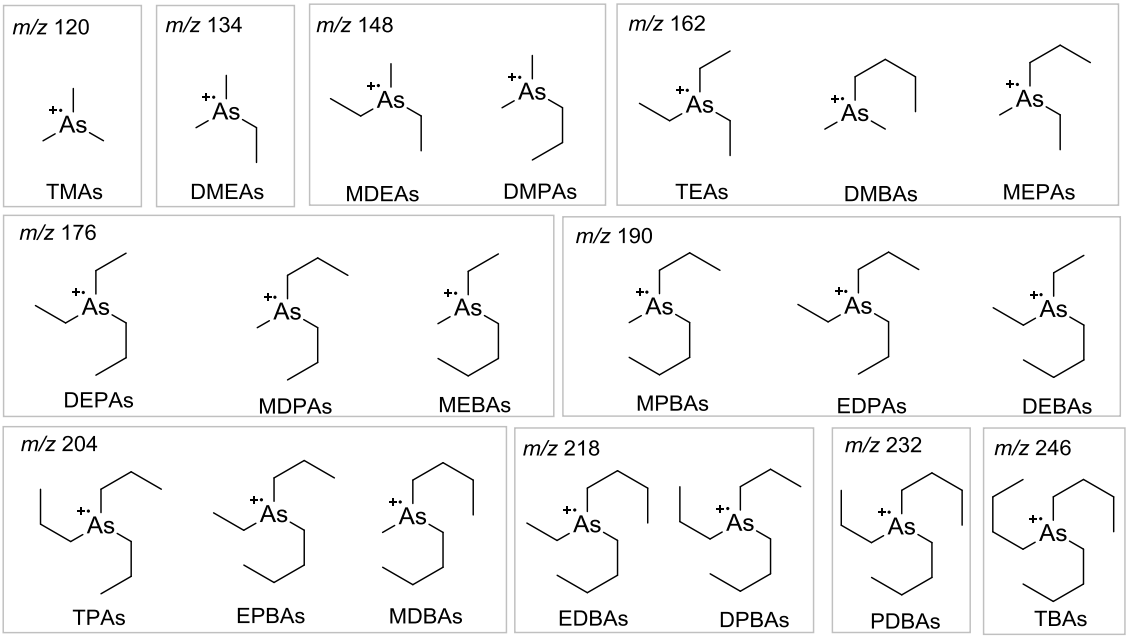

Figure S12. Structures and predicted *m/z* for the synthesized arsines.

AsC_3H_9, trimethyl arsine (TMAs) *m/z* 120

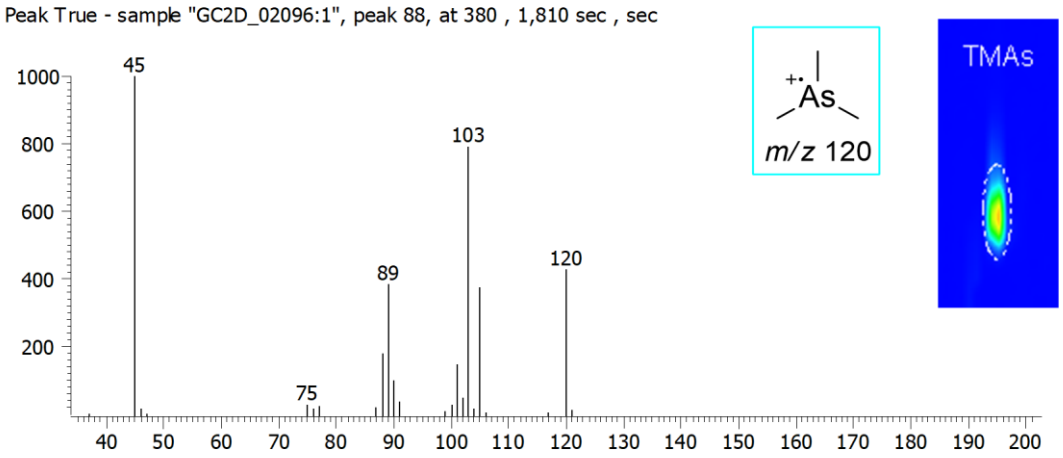

Figure S13. Mass fragmentogram of TMAs (*m/z* 120).

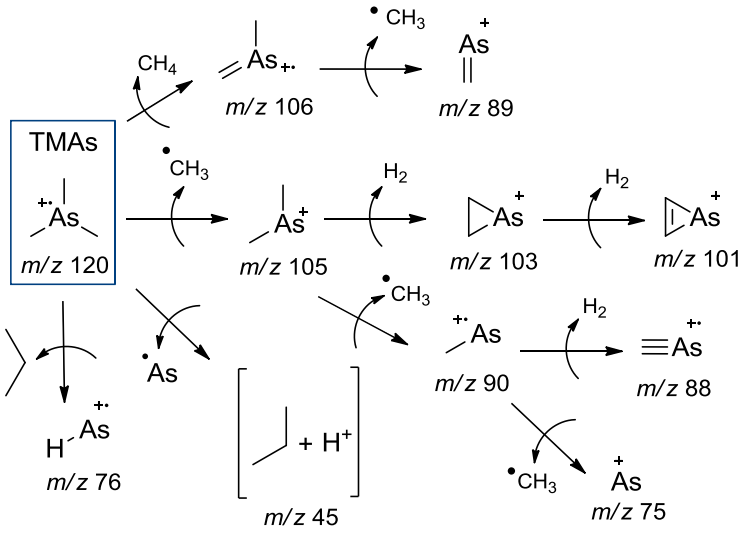

Scheme S5. Proposed fragmentation mechanism for TMAs.

AsC_4H_{11}, dimethylethyl arsine (DMEAs) *m/z* 134

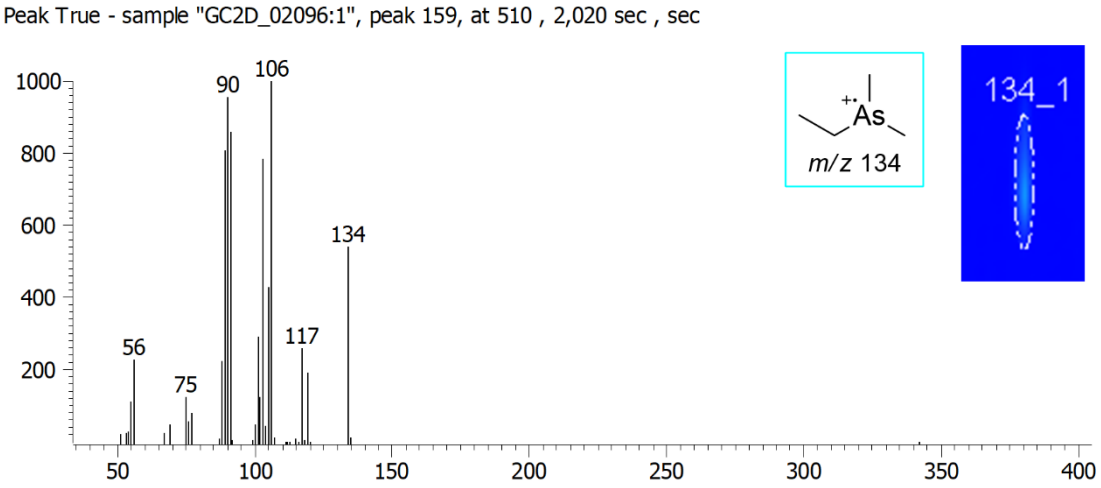

Figure S14. Mass fragmentogram of DMEAs (*m/z* 134).

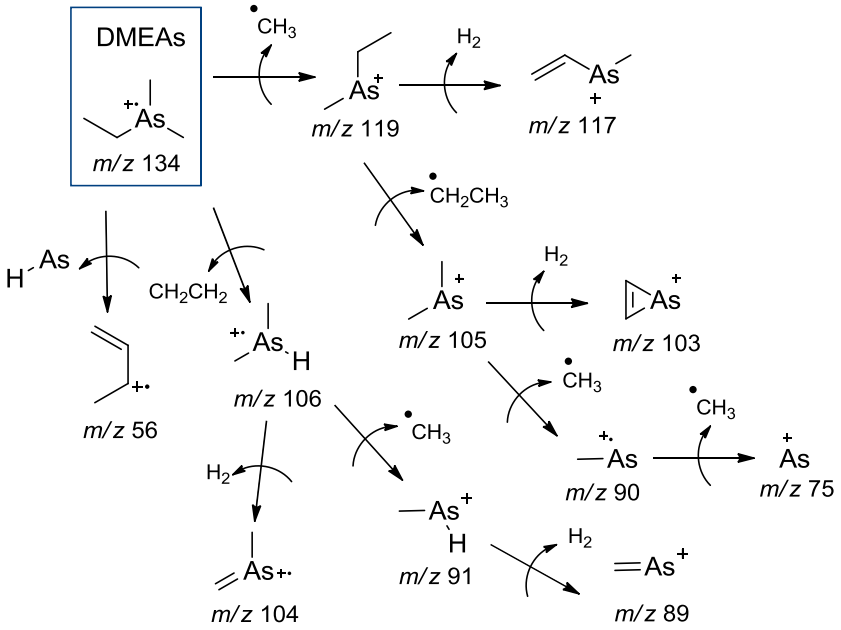

Scheme S6. Proposed fragmentation mechanism for DMEAs.

AsC_5H_{13}, methyldiethyl arsine (MDEAs) *m/z* 148

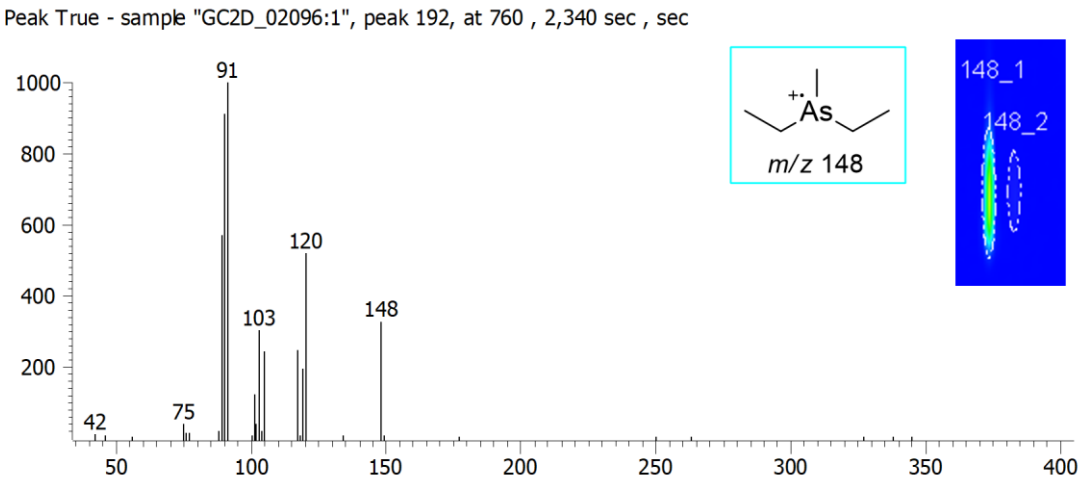

Figure S15. Mass fragmentogram of MDEAs (*m/z* 148).

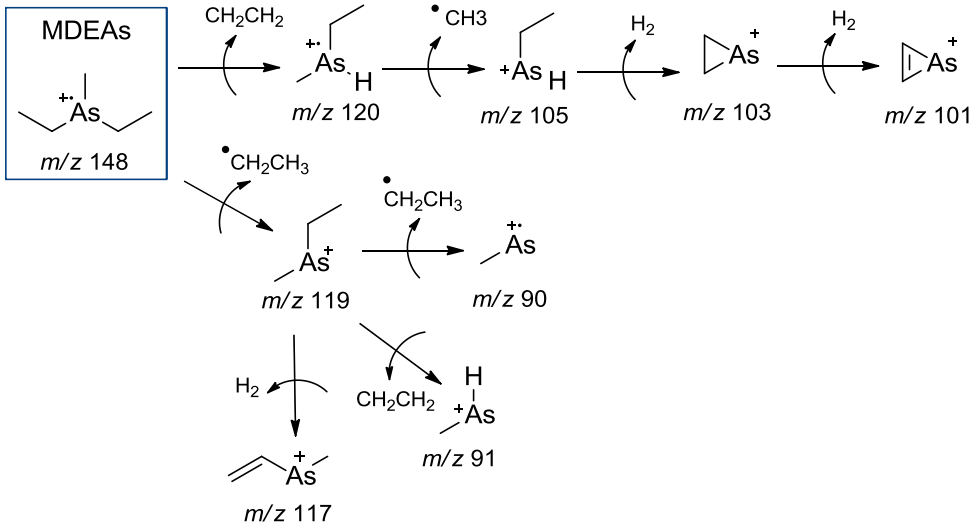

Scheme S7. Proposed fragmentation mechanism for MDEAs.

AsC_5H_{13}, dimethylpropyl arsine (DMPAs) *m/z* 148

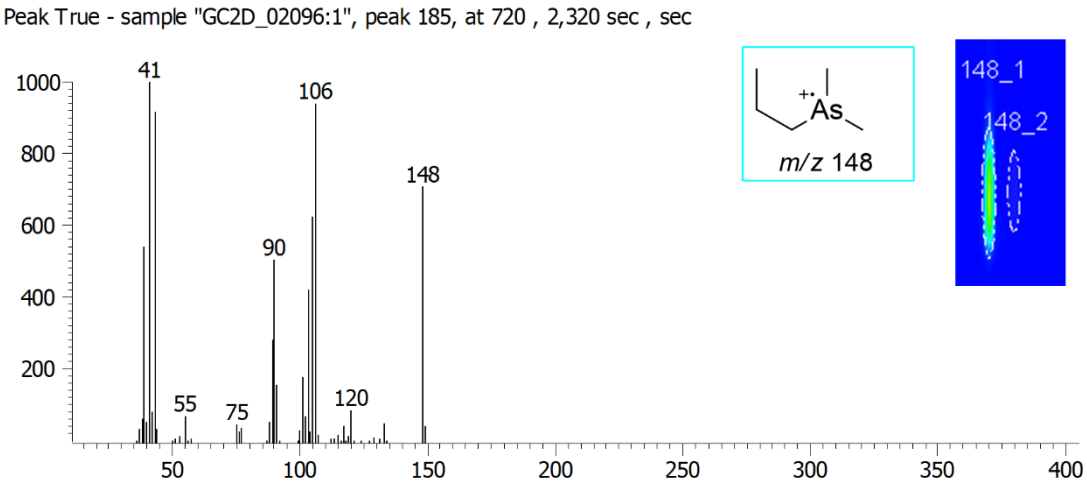

Figure S16. Mass fragmentogram of DMPAs (*m/z* 148).

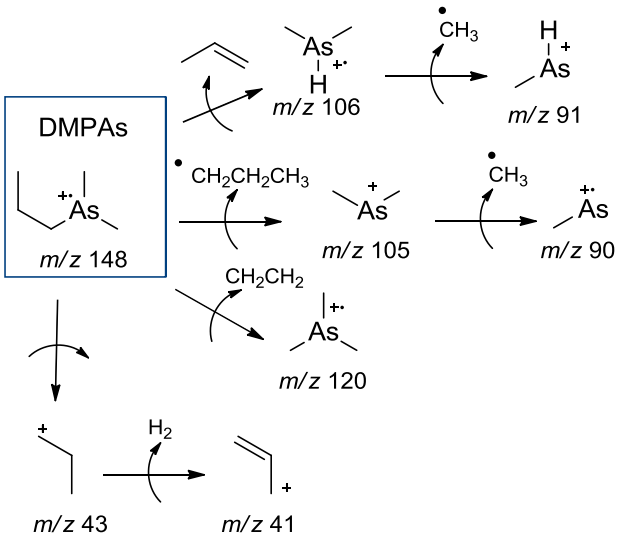

Scheme S8. Proposed fragmentation mechanism for DMPAs.

AsC_6H_{15}, triethyl arsine (TEAs) *m/z* 162

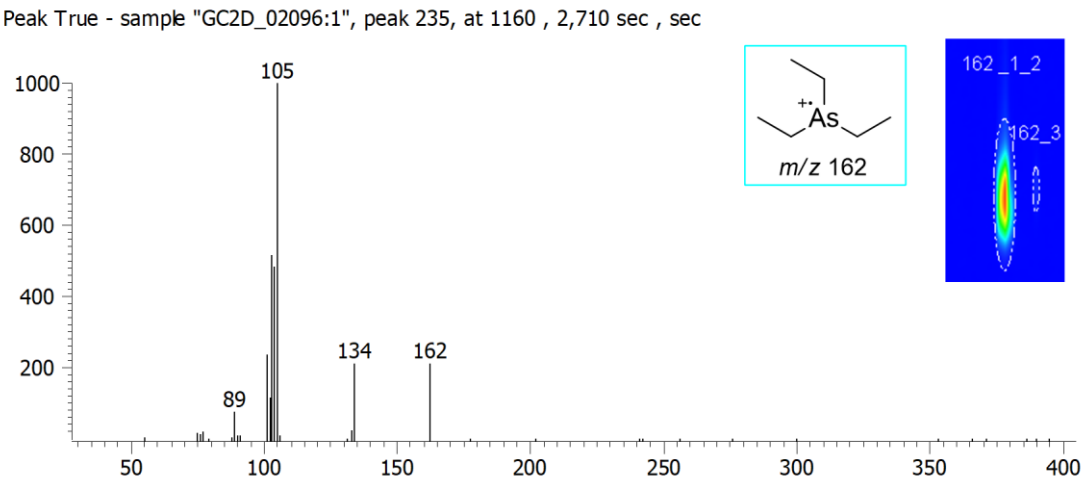

Figure S17. Mass fragmentogram of TEAs (*m/z* 162).

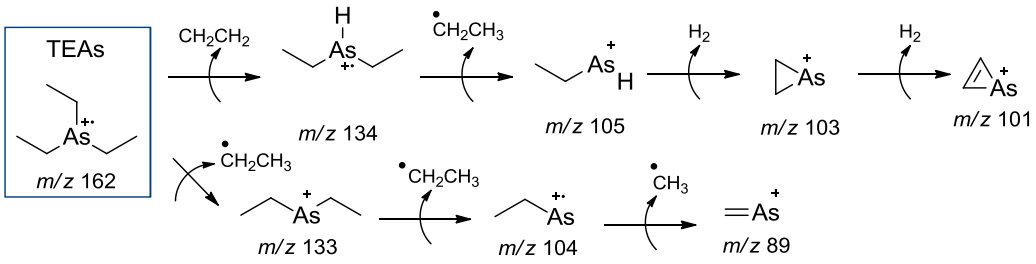

Scheme S9. Proposed fragmentation mechanism for TEAs.

AsC_6H_{15}, dimethylbutyl arsine (DMBAs) *m/z* 162

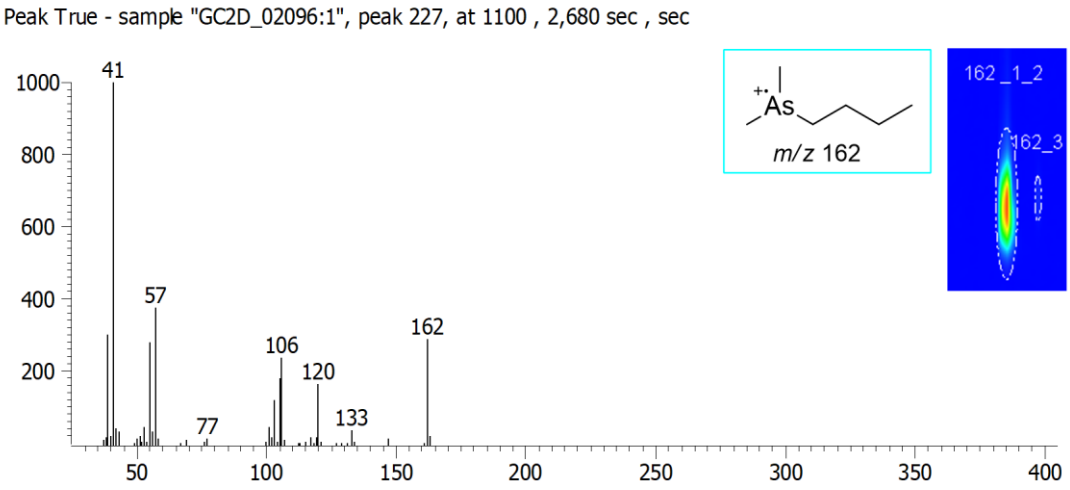

Figure S18. Mass fragmentogram of DMBAs (*m/z* 162).

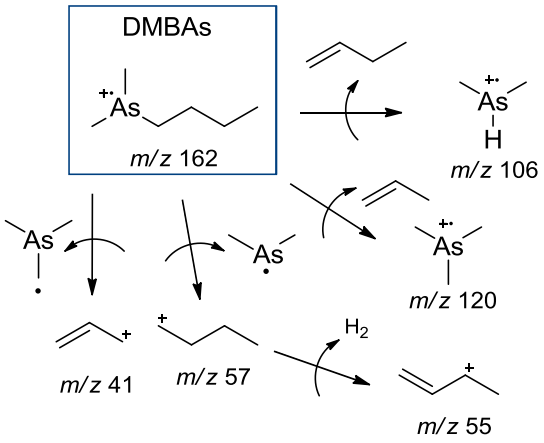

Scheme S10. Proposed fragmentation mechanism for DMBAs.

AsC_6H_{15}, Methylethylpropyl arsine (MEPAs) *m/z* 162

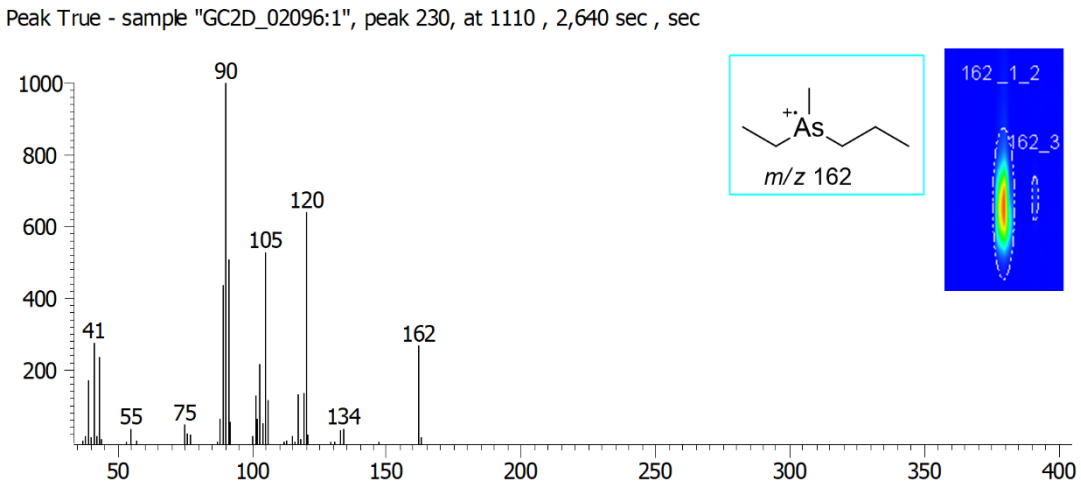

Figure S19. Mass fragmentogram of MEPAs (*m/z* 162).

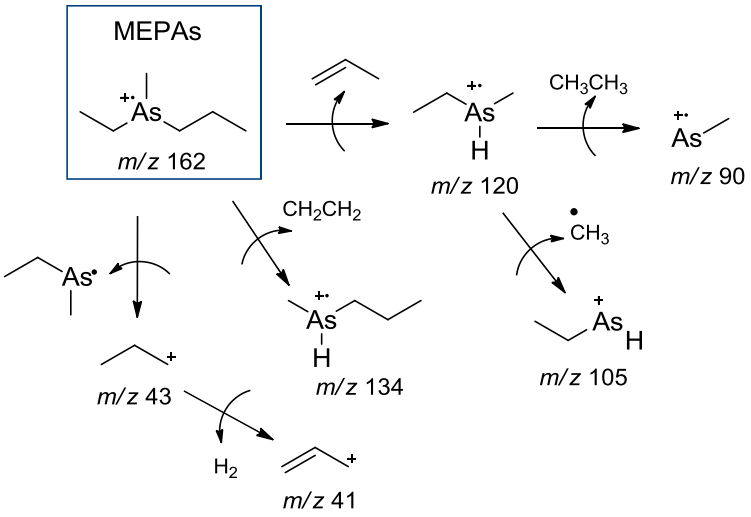

Scheme S11. Proposed fragmentation mechanism for MEPAs.

AsC_7H_{17}, diethylpropyl arsine (DEPAs) *m/z* 176

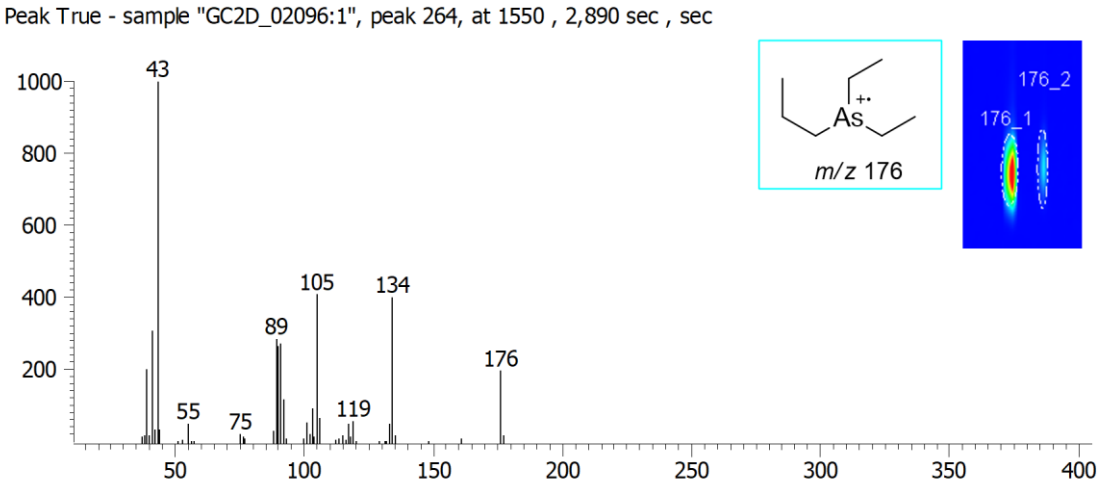

Figure S20. Mass fragmentogram of DEPAs (*m/z* 176).

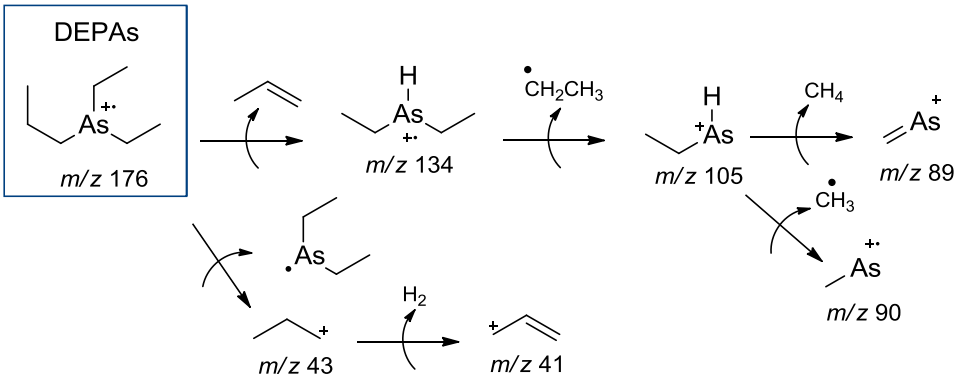

Scheme S12. Proposed fragmentation mechanism for DEPAs.

AsC_7H_{17}, methylethylbutyl arsine (MEBAs) *m/z* 176

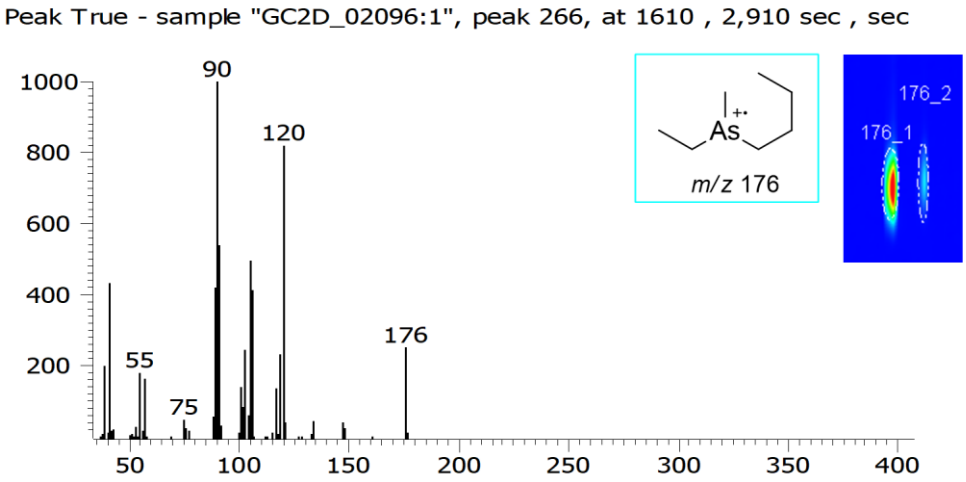

Figure S21. Mass fragmentogram of MEBAs (*m/z* 176).

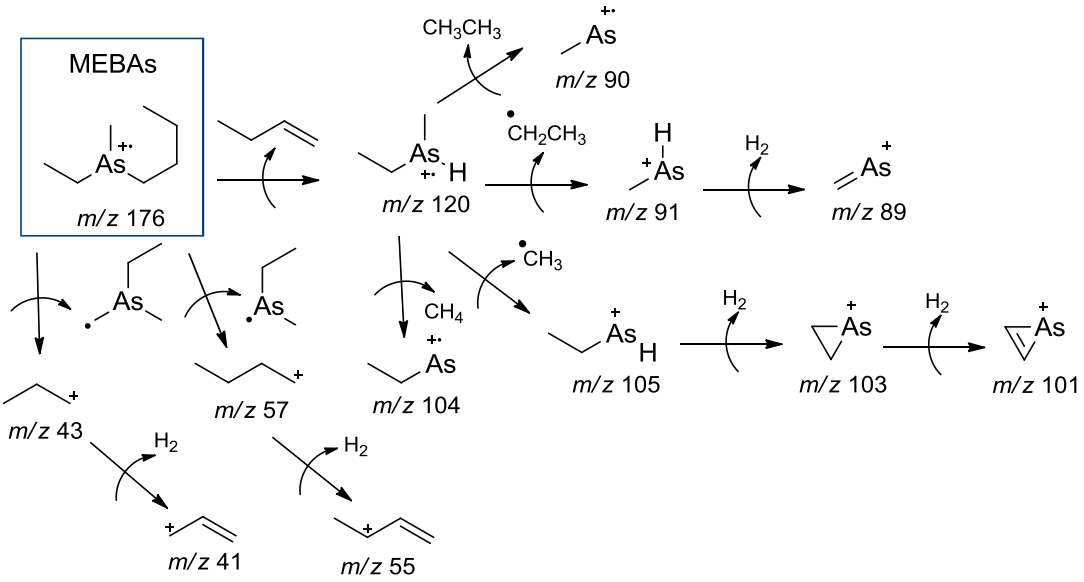

Scheme S13. Proposed fragmentation mechanism for MEBAs.

AsC_8H_{19}, methylpropybutyl arsine (MPBAs) *m/z* 190

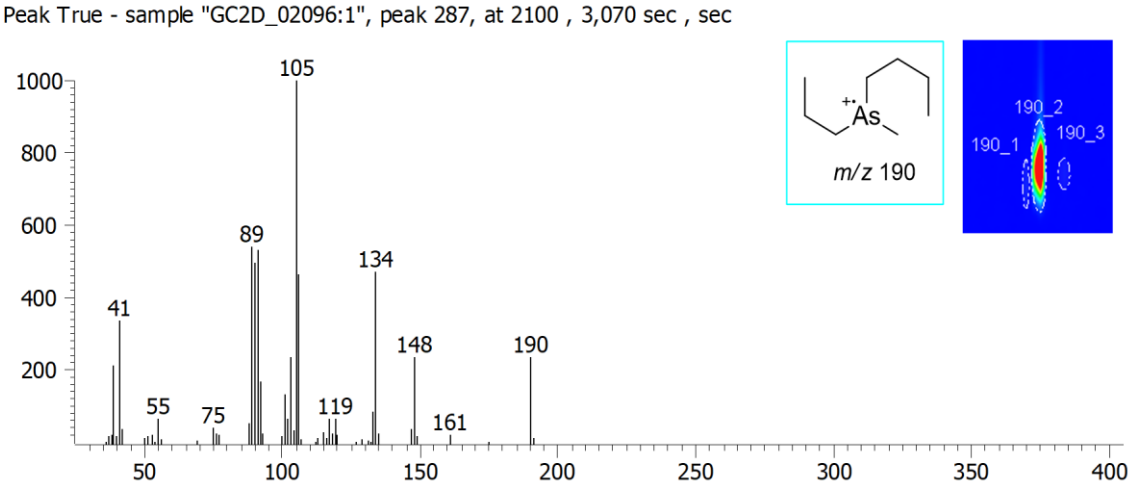

Figure S22. Mass fragmentogram of MPBAs (*m/z* 190).

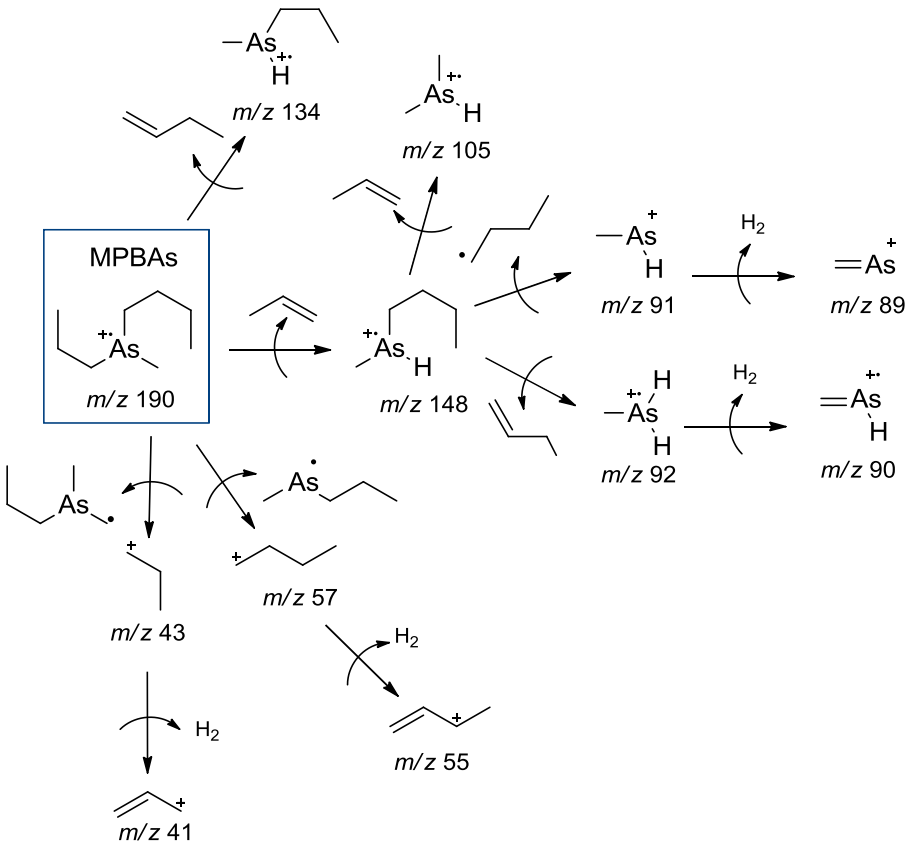

Scheme S14. Proposed fragmentation mechanism for MPBAs.

AsC_8H_{19}, ethyldipropyl arsine (EDPAs) *m/z* 190

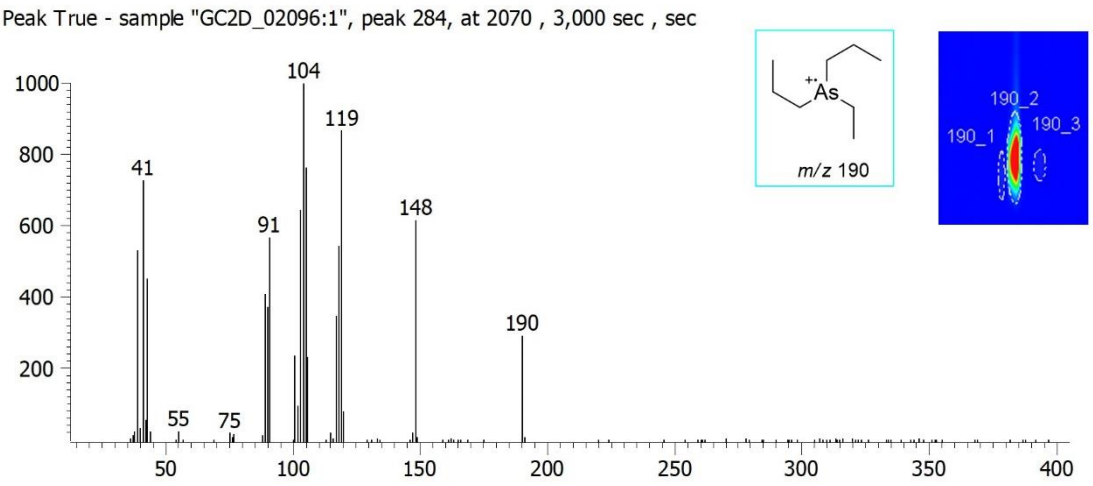

Figure S23. Mass fragmentogram of EDPAs (*m/z* 190).

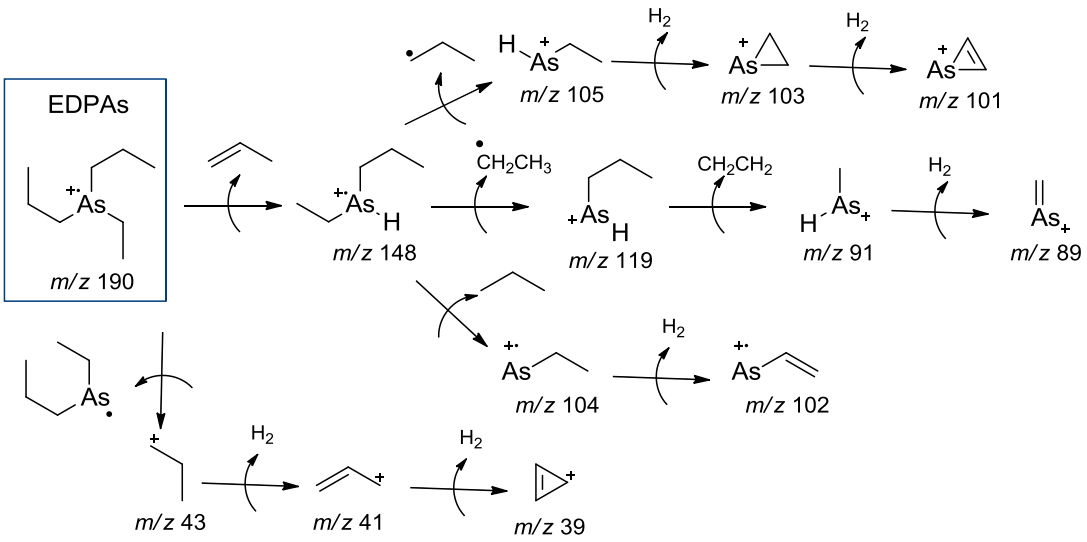

Scheme S15. Proposed fragmentation mechanism for EDPAs.

AsC_8H_{19}, diethylbutyl arsine (DEBAs) *m/z* 190

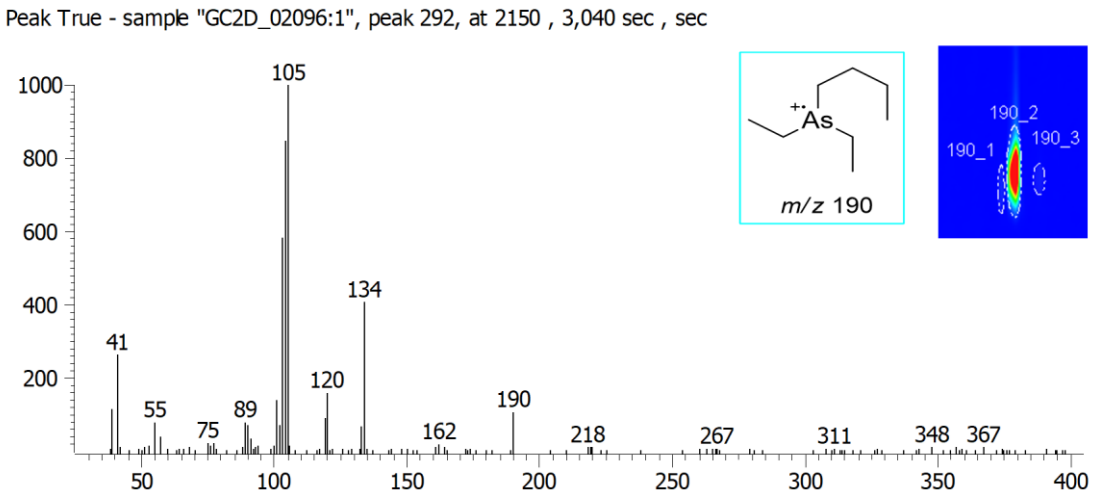

Figure S24. Mass fragmentogram of DEBAs (*m/z* 190).

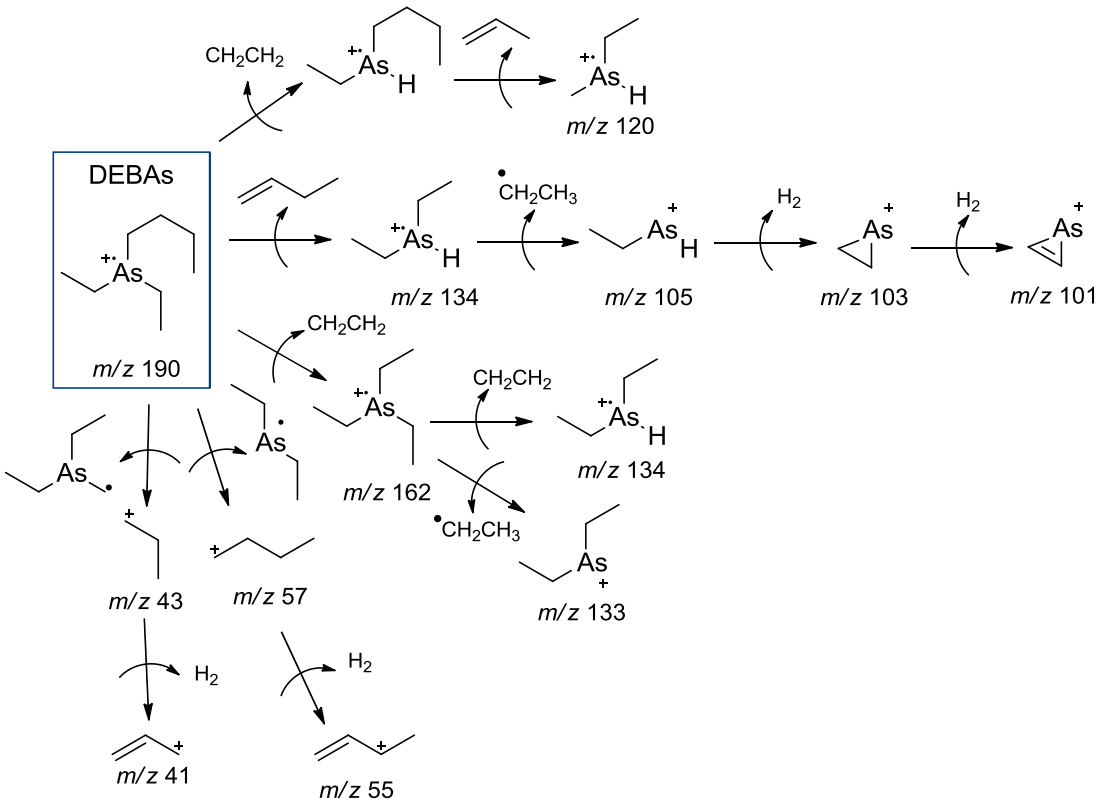

Scheme S16. Proposed fragmentation mechanism for DEBAs.

AsC_9H_{21}, tripropyl arsine (TPAs) *m/z* 204

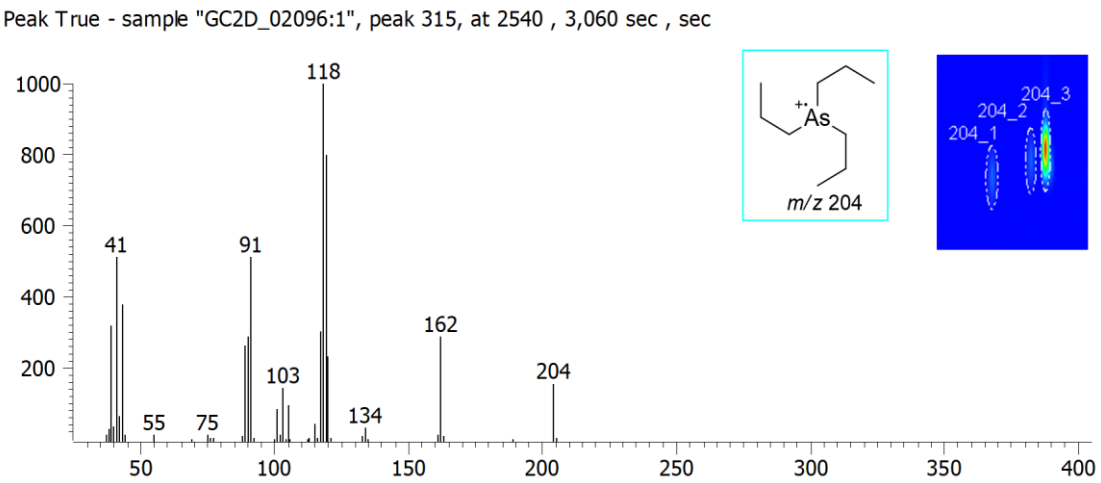

Figure S25. Mass fragmentogram of TPAs (*m/z* 204).

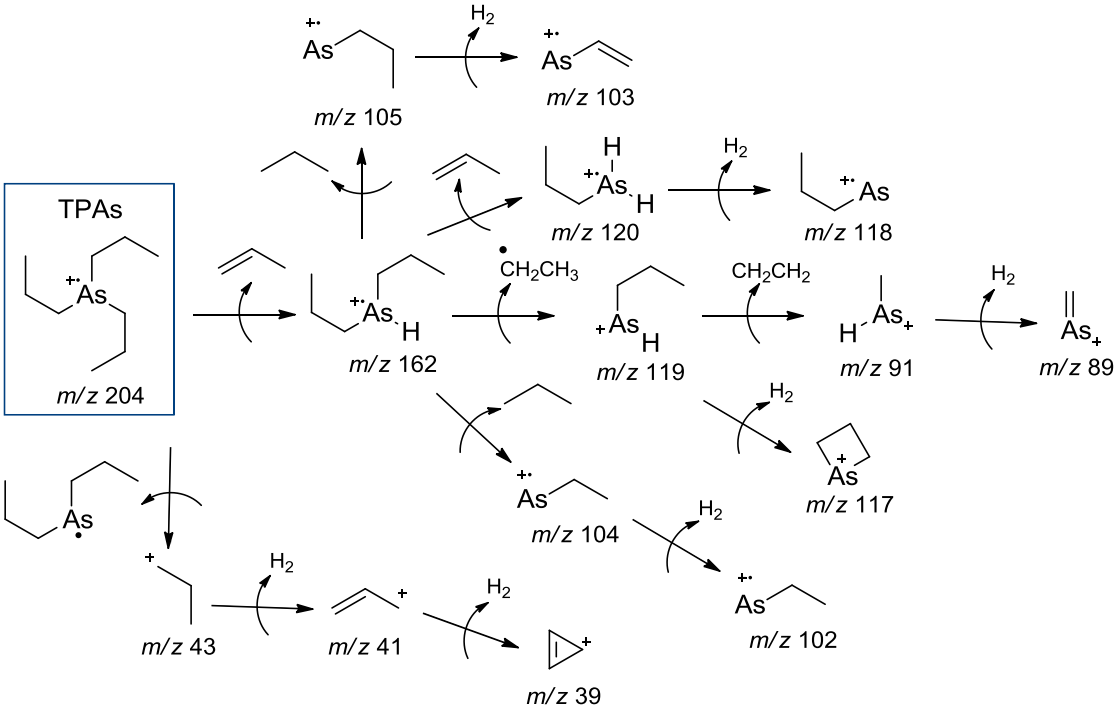

Scheme S17. Proposed fragmentation mechanism for TPAs.

AsC_9H_{21}, methyldibutyl arsine (MDBAs) *m/z* 204

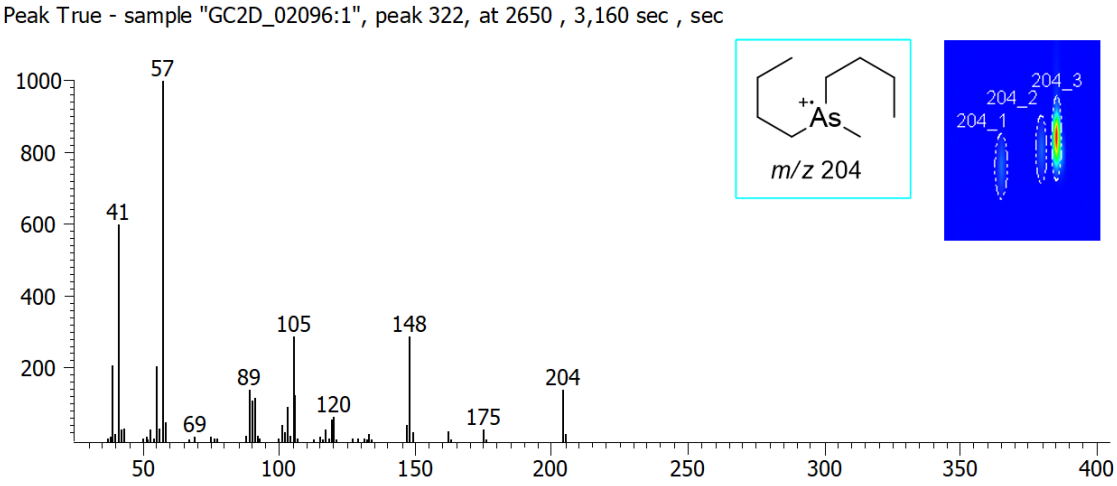

Figure S26. Mass fragmentogram of MDBAs (*m/z* 204).

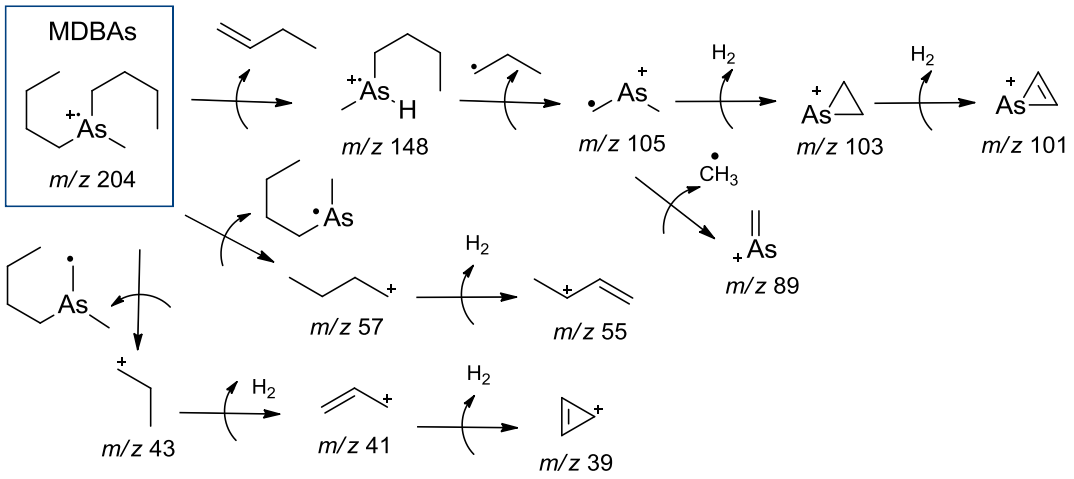

Scheme S18. Proposed fragmentation mechanism for MDBAs.

AsC_9H_{21}, ethylpropylbutyl arsine (EPBAs) *m/z* 204

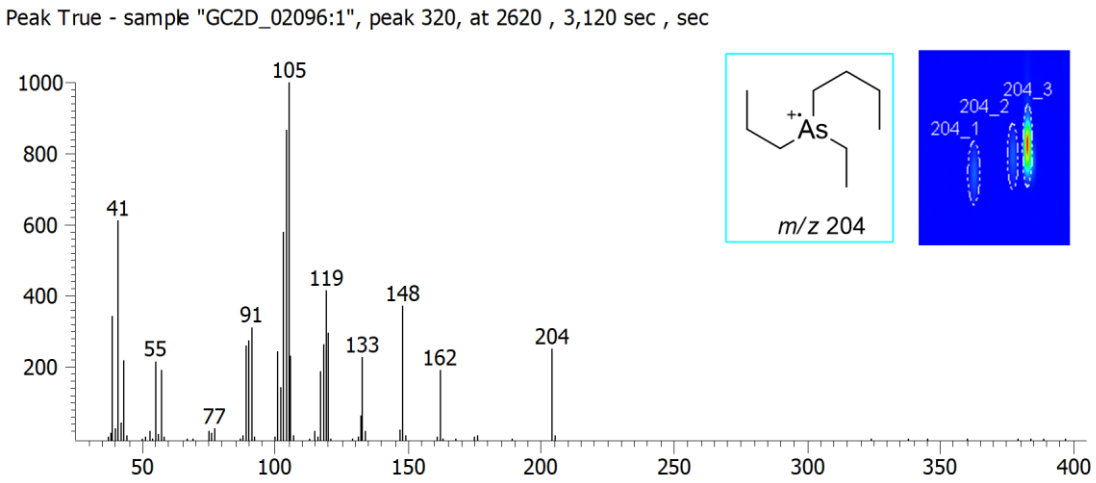

Figure S27. Mass fragmentogram of EPBAs (*m/z* 204).

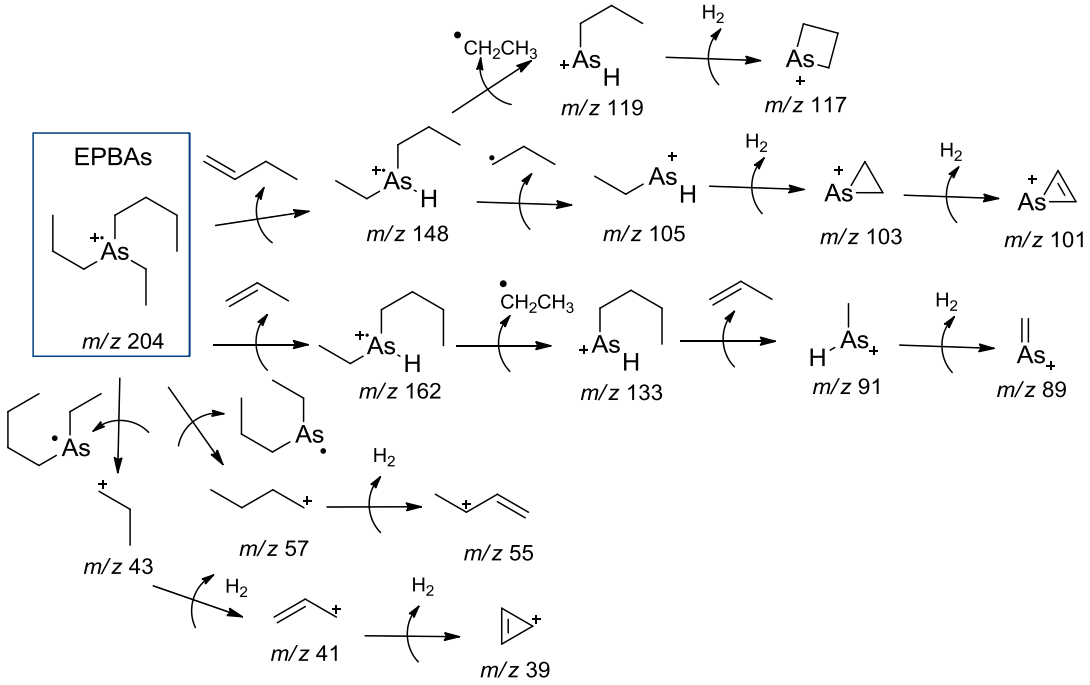

Scheme S19. Proposed fragmentation mechanism for EPBAs.

$AsC_{10}H_{23}$, ethyldibutyl arsine (EDBAs) *m/z* 218

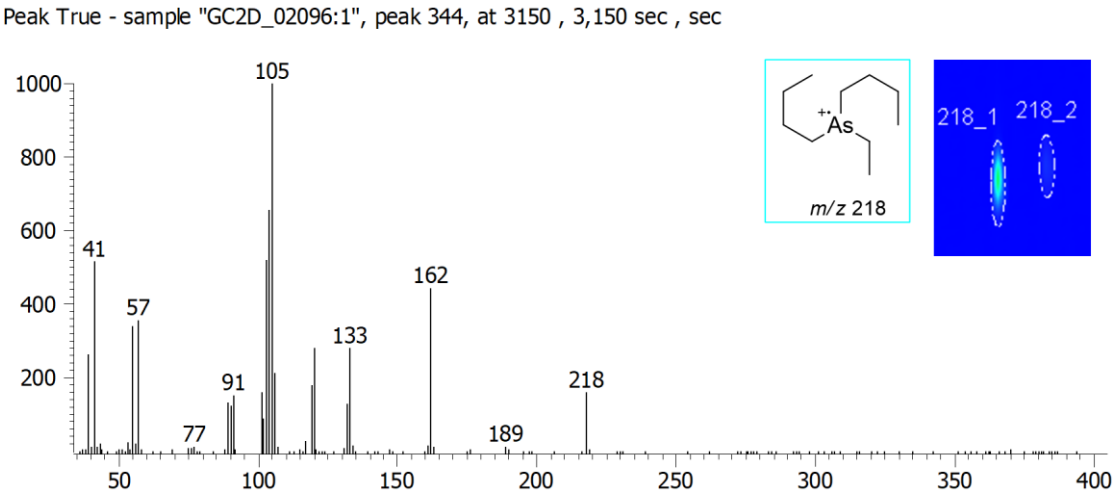

Figure S28. Mass fragmentogram of EDBAs (*m/z* 218).

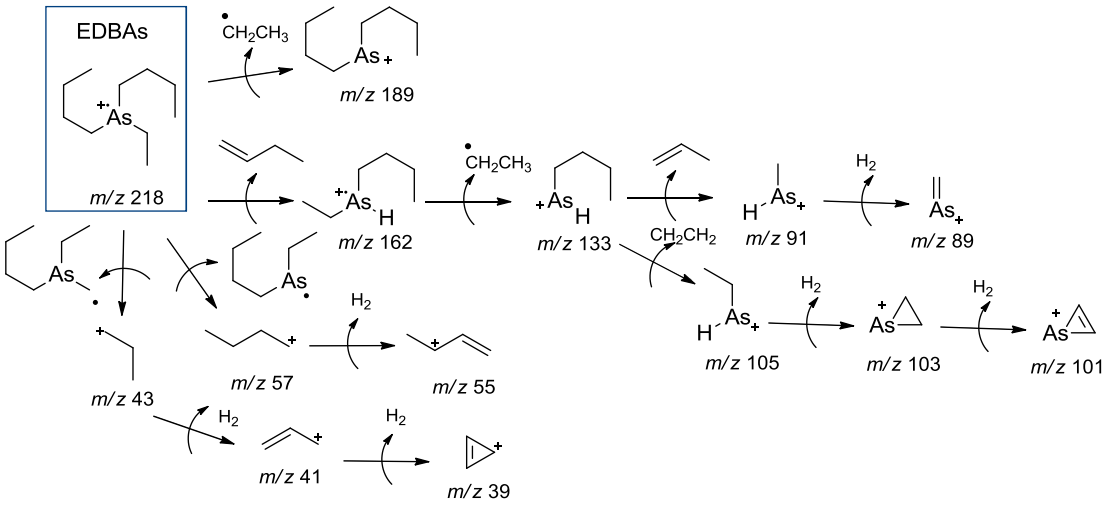

Scheme S20. Proposed fragmentation mechanism for EDBAs.

$AsC_{10}H_{23}$, dipropylbutyl arsine (DPBAs) *m/z* 218

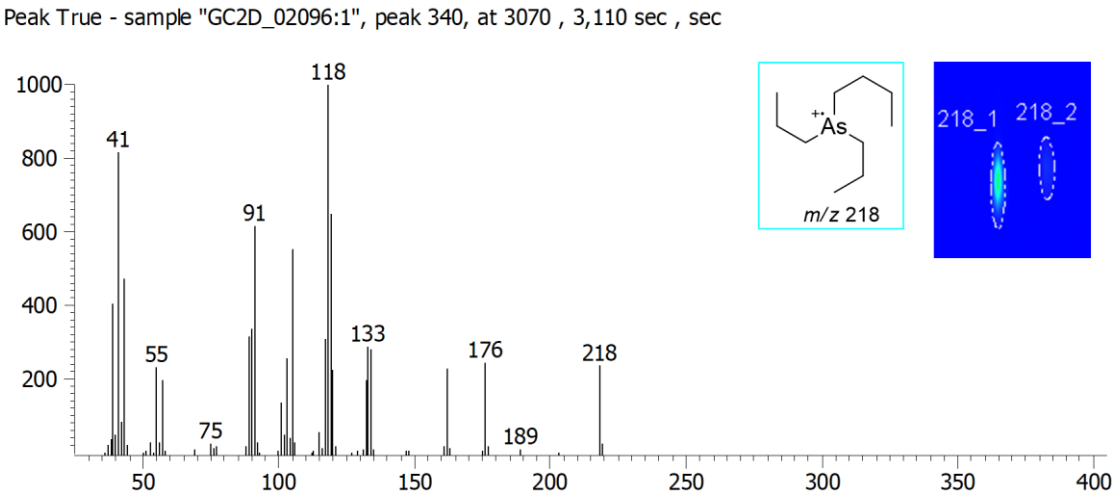

Figure S29. Mass fragmentogram of DPBAs (*m/z* 218).

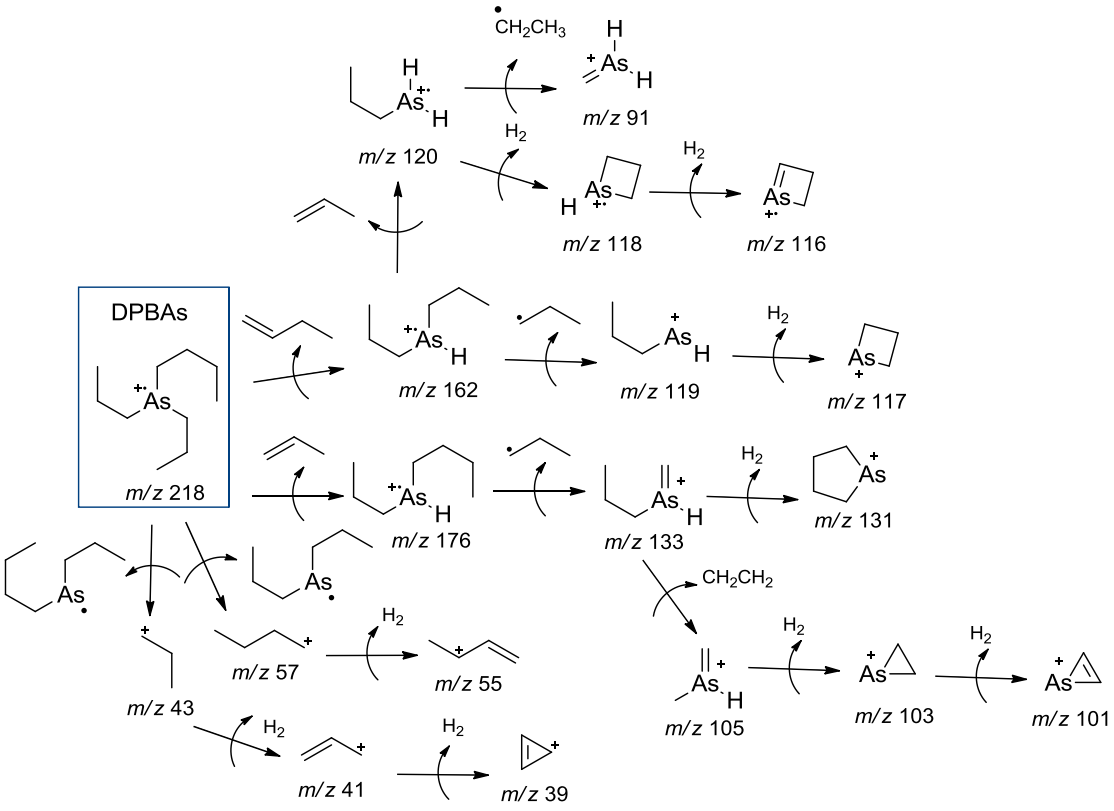

Scheme S21. Proposed fragmentation mechanism for DPBAs.

$AsC_{11}H_{25}$, propyldibutyl arsine (PDBAs) *m/z* 232

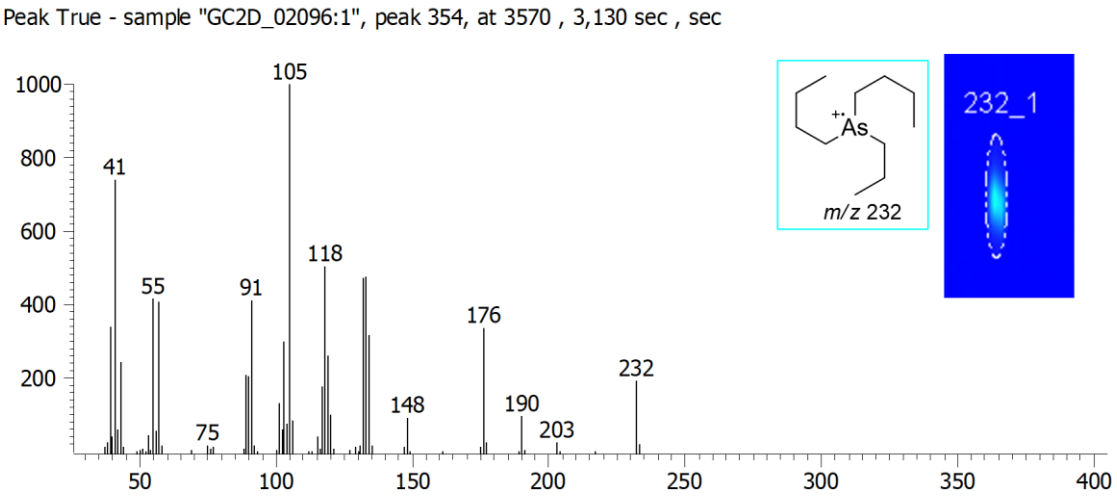

Figure S30. Mass fragmentogram of PDBAs (*m/z* 232).

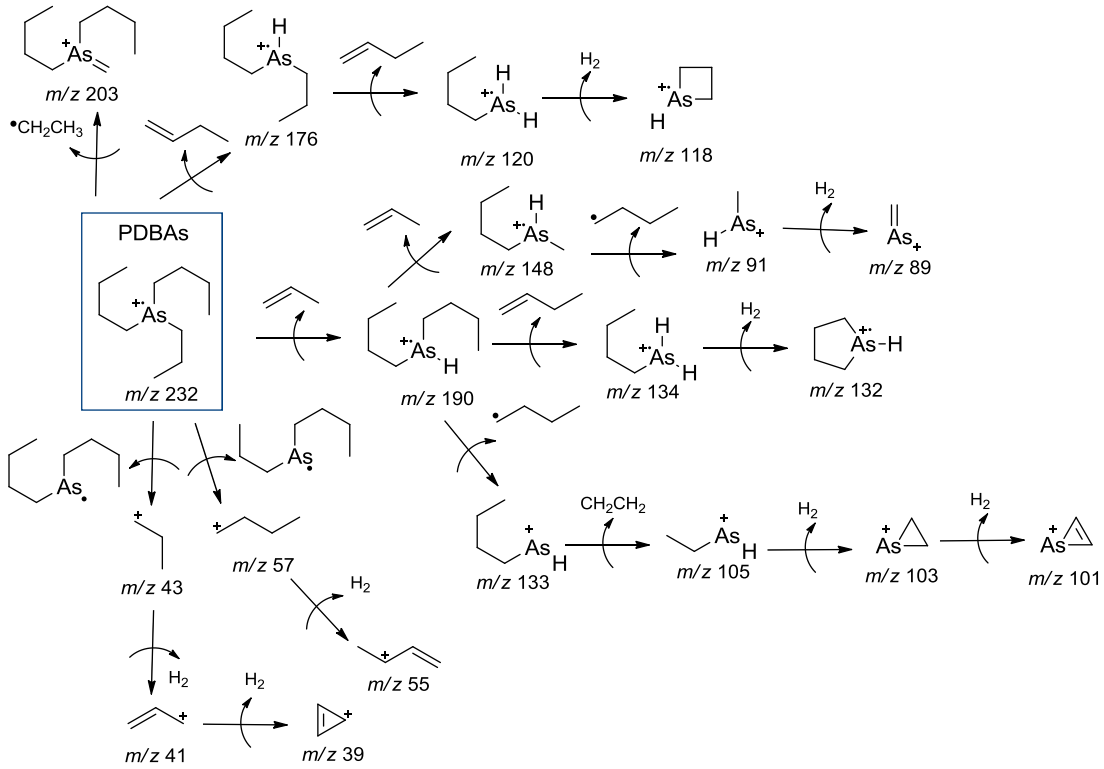

Scheme S22. Proposed fragmentation mechanism for PDBAs.

$AsC_{12}H_{27}$, tributyl arsine (TBAs) *m/z* 246

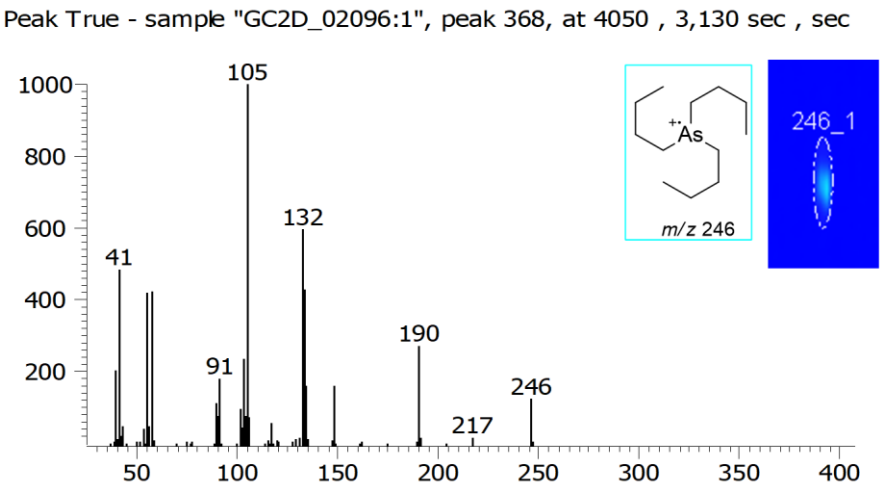

Figure S31. Mass fragmentogram of TBAs (*m/z* 246).

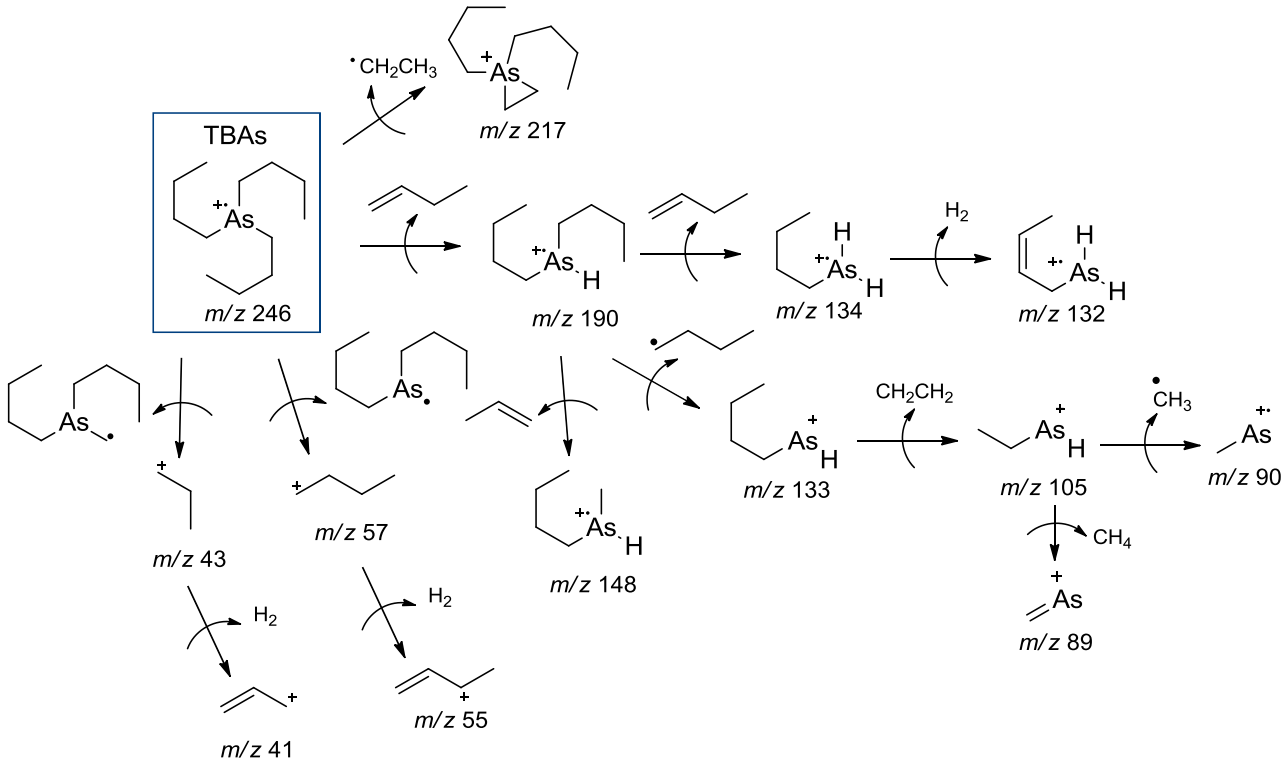

Scheme S23. Proposed fragmentation mechanism for TBAs.

References

1. Enjalbert, R.; Galy, J.; *Acta Crystallogr. B* **1980**, *36*, 914.
2. Spek, A. L.; *Acta Crystallogr. D* **2009**, *65*, 148.
3. Cambridge Crystallographic Data Center (CCDC), 12 Union Road, Cambridge CB2 1EZ, UK, deposit@ccdc.cam.ac.uk, www.ccdc.cam.ac.uk/conts/retrieving.html, accessed in December 2020.
4. Turner, M. J.; Mckinnon, J. J.; Wolff, S. K.; Grimwood, D. J.; Spackman, P. R.; Jayatilaka, D.; Spackman, M. A.; *CrystalExplorer17*; The University of Western Australia, Australia, 2017.